Published in final edited form as:
J Am Soc Mass Spectrom. 2013 November ; 24(11): . doi:10.1007/s13361-013-0700-3.

Electron Capture Dissociation of Divalent Metal-adducted Sulfated *N*-Glycans Released from Bovine Thyroid Stimulating Hormone

Wen Zhou[1,2] and **Kristina Håkansson**[1]
[1]Department of Chemistry, University of Michigan, Ann Arbor, MI 48109-1055, USA

Abstract

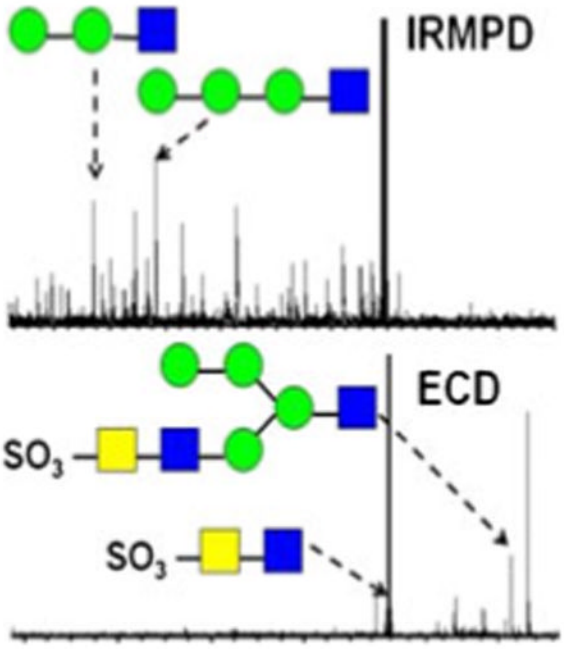

Sulfated *N*-glycans released from bovine thyroid stimulating hormone (bTSH) were ionized with the divalent metal cations Ca^{2+}, Mg^{2+}, and Co by electrospray ionization (ESI). These metal-adducted species were subjected to infrared multiphoton dissociation (IRMPD) and electron capture dissociation (ECD) and the corresponding fragmentation patterns were compared. IRMPD generated extensive glycosidic and cross-ring cleavages, but most product ions suffered from sulfonate loss. Internal fragments were also observed, which complicated the spectra. ECD provided complementary structural information compared with IRMPD, and all observed product ions retained the sulfonate group, allowing sulfonate localization. To our knowledge, this work represents the first application of ECD towards metal-adducted sulfated *N*-glycans released from a glycoprotein. Due to the ability of IRMPD and ECD to provide complementary structural information, the combination of the two strategies is a promising and valuable tool for glycan

Correspondence to: Kristina Håkansson;, kicki@umich.edu.
Present Address: Baxter Healthcare, 1700 Rancho Conejo Blvd, Thousand Oaks, CA 91320, USA

Electronic supplementary material: The online version of this article (doi:10.1007/s13361-013-0700-3) contains supplementary material, which is available to authorized users.

structural characterization. The influence of different metal ions was also examined. Calcium adducts appeared to be the most promising species because of high sensitivity and ability to provide extensive structural information.

Keywords

bTSH; Bovine thyroid stimulating hormone; Oligosaccharides; Glycan; *N*-glycan; Sulfonation; Sulfation; Metal cations; Metal complexes; ECD; Electron capture Dissociation; Fourier transform ion cyclotron resonance; FT-ICR; FTMS; Tandem mass spectrometry; Structural characterization; IRMPD; Infrared multiphoton dissociation

Introduction

Glycosylation is a prevalent protein post-translational modification (PTM), playing key roles in various cellular processes, such as metastasis, cell adhesion, molecular trafficking and clearance, and receptor activation [1–8]. Glycans are assembled in a step-wise fashion by the actions of glycosyltransferases and glycosidases [1], a process which results in highly diverse glycan structures. This structural complexity makes glycan characterization more challenging than the characterization of other linear biomolecules, such as peptides or oligonucleotides. In addition to the sequence of monosaccharides, linkages between the monosaccharides, degrees of branching, and anomericity (α versus β) must be determined to achieve complete characterization of glycans. Mass spectrometry (MS) has been widely applied for the structural determination of glycans due to its ability to offer accurate results, analytical versatility, and high sensitivity (attomole to femtomole range) [9–11]. In particular, Fourier transform ion cyclotron resonance (FT-ICR) MS [12, 13] is a powerful technique because of its high resolution and high mass accuracy [14], and its ability to apply various tandem mass spectrometric (MS/MS) techniques [15].

Structural characterization of sulfated oligosaccharides is a challenging task because of the high lability of the sulfate group. Most MS/MS analysis of sulfated oligosaccharides has been performed in negative ion mode because of the acidity of the sulfate group and its higher stability in the deprotonated state. In particular, collision activated dissociation (CAD) has been extensively applied to characterize sulfated oligosaccharide anions [16–21]. Loss of SO_3 or H_2SO_4 are dominant fragmentation processes in CAD and, thus, localization of sulfate groups is challenging. Choosing a precursor ion of higher charge state, or applying sodium ion exchange, for negative ion CAD analysis can reduce sulfonate elimination [18, 19, 22]. While CAD provides mostly glycosidic cleavages (B-, C-, Y-, and Z-type [23] ions) and some cross-ring cleavages (A- and X-type [23] ions) [16–20], infrared multiphoton dissociation (IRMPD), electron detachment dissociation (EDD) [24–26], and negative electron transfer dissociation (NETD) [27] have been shown to generate extensive cross-ring and glycosidic cleavages in negative ion mode analysis of sulfated glycans and glycosaminoglycans (GAGs) [28–34]. Compared with IRMPD, EDD produces more abundant product ions and reduced sulfonate elimination [30]. However, sulfonate loss is still competing with other fragmentation pathways and, therefore, remains an issue in sulfated oligosaccharide characterization.

In positive ion mode analysis, it has been demonstrated that sulfate groups can be stabilized by forming adducts with alkali and divalent metal cations [35, 36]. It has also been reported that biomolecules coordinated to metal cations provide additional structural information in tandem mass spectrometry compared with their protonated counterparts. For example, CAD of metal-adducted oligosaccharides yielded more extensive cross-ring cleavages than the corresponding protonated species [37–41]. However, the efficiency of CAD decreases with

increasing glycan mass [42]. Alternative MS/MS activation techniques have also been applied for positive ion mode glycan structural analysis, including IRMPD [38, 43–46], high-energy CAD [47–49], 157 nm photodissociation [42, 50, 51], and electron capture dissociation (ECD) [52–56]. The first application of ECD to protonated carbohydrates mainly generated glycosidic cleavages [53]. O'Connor and co-workers observed that ECD of permethylated glycans yielded some unique product ions compared with CAD of the same species [55], illustrating the complementary nature of these two MS/MS techniques in glycan analysis.

The utilization of metals to cationize sulfated glycans has two main advantages: first, divalent metals can stabilize labile sulfate groups [36, 56]. Moreover, divalent metals facilitate the formation of at least doubly positively charged species, which are required for ECD. Our group has previously demonstrated the application of ECD to model oligosaccharides ionized with alkali and divalent metals, and found that complementary structural information was obtained from ECD compared with IRMPD [54]. We also found that ECD of sulfated oligosaccharides ionized with divalent metals provides information about the location of sulfonate groups [56]. However, previous work mainly focused on model oligosaccharides. Here, our objective is to explore the applicability of ECD towards metal-adducted sulfated *N*-glycans released from a glycoprotein, and to compare ECD fragmentation patterns from such branched molecules to those from IRMPD. Divalent metal cations, including Ca^{2+}, Co^{2+}, and Mg^{2+}, were selected as cationizing agents and comparisons were made to determine which metal cation provides the most structural information from IRMPD and ECD. N-linked glycans from bovine thyroid stimulating hormone (bTSH) were released and examined by both techniques.

Experimental

Reagents

Bovine thyroid stimulating hormone and peptide-*N*-glycosidase F (PNGase F) were purchased from Sigma Chemical Co. (St. Louis, MO, USA). Calcium chloride ($CaCl_2$), cobalt(II) bromide ($CoBr_2$), magnesium bromide ($MgBr_2$), ammonium bicarbonate (NH_4HCO_3), and formic acid (HCOOH) were obtained from Fisher (Fair Lawn, NJ, USA). SPE graphitized carbon column was purchased from Alltech Associates Inc. (Deerfield, IL, USA). ZrO_2 microtips were obtained from Glygen Corp. (Columbia, MD, USA).

Preparation of N-Glycans

Ten nmol of bovine thyroid stimulating hormone was denatured at 100 °C for 5 min, then digested with PNGase F (2 U) in 50 mM NH_4HCO_3 (pH 8) overnight at 37 °C. The reaction was halted by heating at 100 °C for 5 min.

Purification and Enrichment of N-Glycans

The released glycans were purified by SPE graphitized carbon column, and then enriched using ZrO_2 microtips. For each sample, a carbon cartridge was washed with 3 mL of 0.1% (vol/vol) formic acid in 80% acetonitrile/H_2O (vol/vol), followed by 3 mL of deionized water. The solution containing *N*-glycans was then loaded followed by washing with 3–5 mL of deionized water to remove salts and other contaminants. The glycans were eluted with 0.5–1 mL of 0.1% formic acid (vol/vol) in 20% acetonitrile/H_2O (vol/vol). The resulting solution was dried down in a vacuum concentrator (Eppendorf, Hamburg, Germany), reconstituted in 10 μL of 3.3% formic acid (binding solution), and loaded onto ZrO_2 microtips equilibrated with the same binding solution. Unbound glycans were removed by washing with 20 μL of H_2O (washing solution), and bound sulfated glycans were eluted with 50 μL of 1% piperidine. The eluted solution was dried down and mixed with $CaCl_2$,

$CoBr_2$, or $MgBr_2$ (final concentration 30–40 μM) in 50% methanol/H_2O (vol/vol) for mass spectrometry analysis.

Mass Spectrometry

All mass spectra were collected with an actively shielded 7-T FT-ICR mass spectrometer with a quadrupole front-end (APEX-Q, Bruker Daltonics, Billerica, MA, USA), as previously described [25]. An indirectly heated hollow dispenser cathode was used to perform ECD [57]. IRMPD was performed with a vertically mounted 25 W, 10.6 μM CO_2 laser (Synrad, Mukilteo, WA, USA). Samples were infused via an Apollo II electrospray ion source at a flow rate of 70 μL/h with the assistance of N_2 nebulizing gas. Following ion accumulation in the first hexapole for 0.05 s, ions were mass selectively accumulated in the second hexapole for 1–4 s. Ions were then transferred through high voltage ion optics and captured with dynamic trapping in an Infinity ICR cell [58]. The accumulation sequence up to the ICR cell fill was looped 4–6 times to optimize precursor ion signal to noise (S/N) ratio. For ECD, the cathode heating current was kept constant at 1.8 A and the cathode voltage was pulsed during the ECD event to a bias voltage of −0.1 to −1.0 V for 50 ms to generate low energy electrons. IRMPD was performed with a laser power of 10 W and with firing times ranging from 40–100 ms. For activated-ion ECD (AI-ECD), *N*-glycan ions were heated with a 10 W (40% power), 20–25 ms IR laser pulse prior to electron irradiation to destroy intramolecular noncovalent interactions [59].

Data Analysis

All mass spectra were acquired with XMASS software (Bruker Daltonics) with 256 data points from *m/z* 100–2000 and summed over 40–64 scans. Data processing was performed with MIDAS software [60]. Time domain data were zero filled once, Hanning apodized, Fourier transformed, and exported to Microsoft Excel for internal frequency-to-mass calibration with a two-term calibration equation [61]. Product ion spectra were interpreted with the aid of the web application GlycoFragment (http://www.glycosciences.de/tools/GlycoFragments/) [62]. Product ions were not assigned unless the S/N ratio was at least 3.

Results and Discussion

All product ions are labeled according to the Domon and Costello nomenclature [23]. Subscript numerals indicate where cleavage occurred and superscript numerals indicate where cross-ring cleavage occurred. When more than one product assignment was possible, all assignments are listed. Internal fragments are indicated by a slash separating the sites of fragmentation (e.g., $Z_{4\beta}/C_5$). For branched oligosaccharides, the letter α represents the largest branch, the letter β represents the second largest branch, and the letter γ represents the third largest branch. N-linked oligosaccharides on bovine TSH were previously examined by Green and co-workers by NMR spectroscopy [63]. The three N-linked glycans investigated here, indicated as glycan 1, glycan 2, and glycan 3, respectively, are shown in Figure 1. Product ions bearing a calcium cation as charge carrier are denoted with a superscript Ca (e.g., C_4^{Ca}). Product ions which underwent sulfonate loss are underlined (e.g., $Y_{3\alpha}^{Ca}$). All three glycans are sulfated hybrid-type *N*-glycans [11].

Fragmentation Behavior of Glycan 1 with Different Metal Adducts in IRMPD and ECD

All selected precursor ions were triply charged with two divalent metal cations (Ca^{2+}, Co^{2+}, or Mg^{2+}) binding to the glycan. Abundant signals were observed for calcium-adducted glycans $(M + 2Ca - H)^{3+}$, indicating that calcium salt is highly effective in ionizing carbohydrates [37, 39]. IRMPD of Ca^{2+} -adducted glycan 1 (Figure 2a) generated glycosidic cleavages between every neighboring monosaccharide, providing rich information regarding sequence and monosaccharide composition. Sulfonate loss was commonly observed in the

spectrum (Supplementary Figure 1a) and, thus, information regarding sulfonate location was absent. Several product ions cannot be distinguished based on their accurate masses, such as $Z_{4\alpha}$ or ($B_4 - SO_3$) and $Y_{4\alpha}$ or ($C_4 - SO_3$). Therefore, both possibilities are included in Supplementary Figure S1a. Several internal fragments resulting from more than one glycosidic cleavage were also generated, such as $(Man)4(GlcNAc)^{Ca}$. Such internal fragments provide additional structural information, but also complicate the spectra. Five cross-ring cleavages were observed following IRMPD, including $^{2,4}A_{2\alpha}$, $^{0,4}A_3$, $^{0,2}A_4$, $^{1,4}A_4$, and $^{0,2}X_1$; $^{0,2}A$, $^{0,4}A$, and $^{2,4}A$-type ions were previously found in CAD and IRMPD (low-energy fragmentation techniques) spectra of glycans [35, 43-54]. The $^{0,2}A_4$ and $^{1,4}A_4$ fragments at the branching point aid the determination of the positions of the glycan antennae. X-type ions can be generated by high-energy CAD [47–49] and 157 nm photodissociation [42, 50, 51] of oligosaccharides, but are not commonly seen following IRMPD.

Figure 2b shows the fragmentation pattern of sulfated glycan 1 following ECD and the corresponding spectrum is shown in Supplementary Figure S1b. All product ions were even-electron ions. Charge-reduced species were not detected, instead proton-stripped species were observed, resulting from gain of an electron and loss of hydrogen. Product ions corresponding to proton-stripped species and neutral loss from the proton-stripped species corresponded to the most abundant peaks in the spectrum. The sulfonate group was retained in all product ions, demonstrating the ability of ECD to retain labile groups. ECD is well-known to have the ability to retain labile PTMs, including phosphorylation, sulfation, and glycosylation [36, 64–67]. Compared with IRMPD, several additional cross-ring cleavages were observed. The product ion at *m/z* 848.7, labeled as loss of 101 Da from the proton-stripped species (Supplementary Figure S1b), can be assigned to several $^{1,3}A$-type ions sharing the same *m/z* ratio, including $^{1,3}A_{1\alpha}$, $^{1,3}A_{2\alpha}$, $^{1,3}A_5$, or $^{1,3}A_6$. The combined $^{1,3}A$- and $^{2,4}A$-type ions from both IRMPD and ECD determine the linkage position of the non-reducing end GlcNAc as the C4-position ($^{1,3}A_{2\alpha}$ and $^{2,4}A_{2\alpha}$). Overall, the combination of IRMPD and ECD data for the calciumadducted *N*-glycan provided extensive structural information.

The IRMPD and AI-ECD fragmentation patterns of the $(M + 2Co - H)^{3+}$ form of glycan 1 are shown in Figure 2c and d, respectively and the corresponding spectra are shown in Supplementary Figure S1c and d. ECD alone generated very little information. Compared with the calcium-adducted species, cobalt adducts generated weaker signal and only one glycosidic cleavage was observed following IRMPD. However, several diagnostic cross-ring cleavage product ions were found only from the cobalt-adducted precursor ion, such as $^{1,3}A_{3\alpha}$, $^{1,3}A_4$, and $^{2,4}A_6$. The two product ions ($^{0,2}A_4$ and $^{1,3}A_4$) at the branching point of the tri-mannose core aid determination of the position of the 3-antenna. This fragmentation pattern is in accordance with an earlier study by Leary and co-workers, who examined the dissociation pathways of Ca^{2+}-, Co^{2+}-, and Mn^{2+}-coordinated oligosaccharides, and found that Co^{2+}-coordinated species exhibited unique fragmentation patterns [39]. In AI-ECD, cobalt adducts yielded three additional glycosidic cleavages ($C_{3\alpha}$, B_5, and C_5) and several additional cross-ring cleavages compared with IRMPD. The peak denoted as $B_5 - 57$ Da (*m/z* 779.2) likely corresponds to loss of C_2H_3NO from *N*-acetylglucosamine (Supplementary Figure S1d). Similar to the calcium adducts, loss of 101 Da from the precursor ion was also observed. The combination of $^{1,3}A_6$ and $^{2,4}A_6$ from AI-ECD of cobalt-adducted glycan 1 determines the linkage position of the GlcNAc at the reducing end. Cross-ring product ions aid linkage type determination, particularly the ones occurring at the branching points. However, the lack of sufficient glycosidic cleavages made the sequencing of this glycan difficult. Therefore, cobalt adducts were not as effective as calcium adducts in achieving extensive structural characterization for sulfated *N*-glycan 1 via IRMPD and ECD.

IRMPD and ECD were also performed for magnesium-adducted glycan 1 $(M + 2Mg - H)^{3+}$. Following IRMPD, glycosidic cleavages between every neighboring monosaccharide and five cross-ring cleavages were observed (Figure 2e and Supplementary Figure S1e). Among the five cross-ring cleavages, three were unique to the IRMPD spectrum of Mg^{2+}-adducted glycan 1 with one of them at the branching point of the tri-mannose core. When product ions cannot be distinguished based on their *m/z* ratio, all possible assignments are included. For example, Z_1 and $B_{1\alpha}$ without a sulfonate attached both correspond to the mass of a HexNAc. Such ambiguous assignments are often a consequence of sulfonate loss from B- or C-type ions. The latter loss was common in product ions generated by IRMPD. However, all assignments in ECD spectra were unambiguous because all product ions retained the sulfonate group.

In contrast to calcium and cobalt adducts, ECD of Mg^{2+}-adducted glycan 1 provided little structural information (data not shown). Only the proton stripped species $(M + 2Mg - 2H)^{2+}$ and loss of 42 Da from the proton stripped species were observed. Loss of 42 Da likely corresponds to loss of a ketene molecule (CH_2CO) from *N*-acetylglucosamine, as previously reported [53, 54]. We observed retention of the sulfonate group in calcium- and cobalt-adducted *N*-glycans following ECD, while IRMPD of metal-adducted glycan 1 showed extensive sulfonate loss (see Supplementary Figure S1a, c, and e). Therefore, magnesium adduction is not favored for glycan 1 because of the difficulties in achieving sulfonate localization and unambiguous fragment assignments.

In addition to the highly complementary fragmentation from IRMPD and ECD described above, it is also of interest to examine quantitative differences in fragments shared between IRMPD and ECD. For calcium-adducted glycan 1, the glycosidic fragments C_4, C_5, and $Y_{4\beta}$ were observed following both IRMPD and ECD (Figure 1a, b, and Supplementary Figure S1a, b). The relative signal abundance of these fragments is, in general, higher following IRMPD because of the higher fragmentation efficiency compared with ECD but presumably also because charge reduction does not necessarily occur in IRMPD. For example, C_5 and $Y_{4\beta}$ are observed in both their triply and doubly charged forms following IRMPD but only as doubly charged (and singly charged for C_5) following ECD, as expected. For cobalt-adducted glycan 1, one glycosidic fragment, C_4, and one cross-ring fragment, $^{2,4}A_6$, were shared between IRMPD and AI-ECD. Triply charged C_4 was observed following IRMPD, whereas the same product was doubly charged following AI-ECD. The same charge difference was noted for $^{2,4}A_6$ although the fragmentation pathway resulting in this product was particularly favored in AI-ECD, which yielded a 17% relative abundance of this cross-ring fragment.

We also attempted to ionize the *N*-glycan with other metal cations, such as Mn^{2+}, Zn^{2+}, Ba^{2+}, and Al^{3+}. However, no metal-adducted glycan was observed in positive ion mode. The lack of adduct formation may be attributed to the ionic radii and coordination numbers of different metal cations [39]. In general, larger metal ions are not favored for glycan fragmentation, probably because it is difficult for large metal cations to assist charge-induced fragmentation [38, 43]. Harvey investigated the ability of divalent metal ions for ionizing carbohydrates and found that calcium is most effective with magnesium, and cobalt being somewhat less effective [37], in accordance with our observations. Although cobalt-coordinated oligosaccharides have shown unique fragmentation pathways in CAD [39, 40], it is not straightforward to form cobalt adducts with the sulfated *N*-glycan examined here compared with calcium adducts. Also, few glycosidic cleavages were observed in both IRMPD and ECD spectra of the cobaltadducted glycan. Therefore, we focused on calcium adducts because of the higher available signal and the ability to generate extensive glycosidic and cross-ring cleavages in IRMPD and ECD.

Fragmentation Behavior of Ca^{2+}-Adducted Glycan 2 in IRMPD and ECD

IRMPD of Ca^{2+}-adducted sulfated glycan 2 $(M + 2Ca - H)^{3+}$ was also performed (Figure 3a). Glycosidic cleavages were generated between every neighboring monosaccharide unit with only one exception. Most of the glycosidic cleavages resulted in B- and C-type ions with low molecular weight, indicating that fragmentation may occur from the non-reducing end of the *N*-glycan. Four cross-ring fragments were seen ($^{0,2}A_{2\alpha}$, $^{2,4}A_{2\alpha}$, $^{0,2}A_{2\beta}$, and $^{0,4}A_4$) with one ($^{0,4}A_4$) at the tri-mannose core branching site, aiding determination of the branch position. Sulfonate loss was observed in most of the product ions, thus precluding localization of the labile sulfonate group. It is difficult to localize where the two Ca^{2+} ions bind based on the product ion assignments. Lebrilla and co-workers investigated the coordination of alkali metal ions to oligosaccharides by calculating multicollision dissociation threshold (MCDT) values and by molecular dynamics, and predicted that metal ions coordinate at or near glycosidic oxygen(s) [38]. Most product ions bearing two calcium cations retained the sulfonate group, whereas most product ions that lost the sulfonate group bore only one calcium cation. Therefore, we believe one of the Ca^{2+} ions likely binds to the acidic sulfonate group, while the other one coordinates with one or more glycosidic oxygen(s).

In the ECD spectrum of $(M + 2Ca - H)^{3+}$ (Figure 3b), fewer fragments were observed compared with IRMPD because of the lower fragmentation efficiency of ECD [57]. However, two product ions unique to ECD provided additional structural information compared with IRMPD. In order to break noncovalent interactions within this *N*-glycan and thus improve fragmentation efficiency, AI-ECD [59] was applied. Following AI-ECD (Figure 3c), three additional product ions (B_5, $C_{2\alpha}$, and $^{2,4}A_5$) were detected compared with ECD alone, demonstrating improved fragmentation efficiency. In contrast to IRMPD, ECD mainly produced large fragments containing the reducing end, indicating that charge neutralization occurs remote from the reducing end of the *N*-glycan. Our previous study on model oligosaccharides showed similar fragmentation behavior [54]. Moreover, all product ions from AI-ECD were completely different from the ones observed in IRMPD, thereby generating truly complementary structural information (Scheme 1a and b). The complementary capabilities of IRMPD and ECD for biomolecular structural analysis have previously been applied to a variety of biomolecules, including peptides [64], oligosaccharides [54–56], oligonucleotides [68, 69], and proteins [70]. Our results demonstrate that the combination of IRMPD and ECD is also a promising tool for structural characterization of released sulfated *N*-glycans.

Fragmentation Behavior of Ca^{2+}-Adducted Glycan 3 in IRMPD and ECD

IRMPD and ECD fragmentation patterns for calciumadducted glycan 3 are shown in Figure 4a and b, respectively, and the corresponding spectra are shown in Supplementary Figure S2. In the IRMPD spectrum, the most abundant fragment is assigned as Y_γ^{2Ca} (*m/z* 545.8), corresponding to loss of a fucose residue from the core structure. The fucose glycosidic bond is highly labile and dominant fucose loss has been previously observed [71]. Except for Y_γ^{2Ca}, all other glycosidic cleavages resulted in B- and C-type ions. In addition to six glycosidic cleavages, three cross-ring cleavages were found, with one of them ($^{0,4}A_4$) occurring at the trimannose branching site. This result verifies that IRMPD of sulfated *N*-glycans can provide rich structural information.

Following ECD, the fragment corresponding to fucose loss was not detected. In addition, sulfonate loss from the product ions was absent. The preservation of labile bonds demonstrates that ECD proceeds through a different mechanism compared with IRMPD and thus provides complementary structural information. Similar to ECD of glycan 2, no charge-reduced species were found. Instead, proton-stripped species and loss of 42 Da from the

proton-stripped species were observed with high relative abundance. Compared with IRMPD, fewer product ions were observed. However, the fragment at *m/z* 737.7 ($^{2,4}A_6^{2Ca}$) was only found following ECD, demonstrating the ability of ECD to provide additional information in comparison with IRMPD.

Conclusion

We have demonstrated the first application of metal-assisted ECD towards sulfated N-linked glycans released from glycoproteins. Influence of different divalent metal cations such as Ca^{2+}, Mg^{2+}, and Co^{2+} was investigated, and calcium adducts were found as the most promising species because of high signal abundance and ability to provide extensive glycosidic and cross-ring cleavages following both IRMPD and ECD. Co^{2+}-adducted glycans generated some unique product ions. However, in both IRMPD and ECD of cobaltadducted species, cross-ring fragments were predominant and the lack of glycosidic cleavages significantly increased the difficulty of glycan sequencing. Mg^{2+}-adducted glycans provided rich structural information following IRMPD, including both glycosidic cleavages and some cross-ring cleavages. However, ECD of magnesium-adducted glycans generated few fragments, thus making sulfonate localization difficult. Therefore, we believe that calcium-assisted IRMPD and ECD provide the most structural information for sulfated *N*-glycans.

IRMPD and ECD were applied to several sulfated *N*-glycans released from bTSH. IRMPD of Ca^{2+}-adducted glycans produced extensive glycosidic cleavages and several cross-ring cleavages at the branching point. However, most product ions underwent sulfonate loss. Therefore, it is difficult to determine the position of the sulfonate group. ECD of Ca^{2+}-adducted glycans yielded unique product ions in comparison with IRMPD, thus providing complementary structural information. Moreover, all product ions observed in ECD spectra retained the sulfonate group, which is crucial to sulfonate localization. The complementary ability of IRMPD and ECD makes the combination of these two MS/MS techniques a powerful tool in sulfated *N*-glycan structural analysis.

Supplementary Material

Refer to Web version on PubMed Central for supplementary material.

Acknowledgments

This work was supported by Award Number R21CA138331 from the National Cancer Institute. The content is solely the responsibility of the authors and does not necessarily represent the official views of the National Cancer Institute or the National Institutes of Health. W.Z. was partially supported by a George Ashworth Analytical Chemistry Fellowship from the University of Michigan.

References

1. Bertozzi CR, Kiessling LL. Chemical glycobiology. Science. 2001; 291:2357–2364. [PubMed: 11269316]
2. Rudd PM, Elliott T, Cresswell P, Wilson IA, Dwek RA. Glycosylation and the Immune System. Science. 2001; 291:2370–2376. [PubMed: 11269318]
3. Ohtsubo K, Marth JD. Glycosylation in cellular mechanisms of health and disease. Cell. 2006; 126:855–867. [PubMed: 16959566]
4. Dube DH, Bertozzi CR. Glycans in cancer and inflammation. Potential for therapeutics and diagnostics. Nat Rev Drug Disc. 2005; 4:477–488.
5. Lowe JB, Marth JD. A genetic approach to mammalian glycan function. Annu Rev Biochem. 2003; 72:643–691. [PubMed: 12676797]

6. Pilobello KT, Mahal LK. Deciphering the glycocode: the complexity and analytical challenge of glycomics. Curr Opin Chem Biol. 2007; 11:300–305. [PubMed: 17500024]
7. Zhao YY, Takahashi M, Gu JG, Miyoshi E, Matsumoto A, Kitazume S, Taniguchi N. Functional roles of *N*-glycans in cell signaling and cell adhesion om cancer. Cancer Sci. 2008; 99:1304–1310. [PubMed: 18492092]
8. Varki A. Biological roles of oligosaccharides—all of the theories are correct. Glycobiology. 1993; 3:97–130. [PubMed: 8490246]
9. Zaia J. Mass spectrometry of oligosaccharides. Mass Spectrom Rev. 2004; 23:161–227. [PubMed: 14966796]
10. Harvey DJ. Matrix-assisted laser desorption/ionization mass spectrometry of carbohydrates. Mass Spectrom Rev. 1999; 18:349–450. [PubMed: 10639030]
11. Mechref Y, Novotny MV. Structural investigations of glycoconjugates at high sensitivity. Chem Rev. 2002; 102:321–369. [PubMed: 11841246]
12. Marshall AG, Hendrickson CL, Jackson GS. Fourier Transform ion cyclotron resonance mass spectrometry: a primer. Mass Spectrom Rev. 1998; 17:1–35. [PubMed: 9768511]
13. Marshall AG, Hendrickson CL. High-resolution mass spectrometers. Annu Rev Anal Chem. 2008; 1:579–599.
14. Park YM, Lebrilla CB. Application of Fourier transform ion cyclotron resonance mass spectrometry to oligosaccharides. Mass Spectrom Rev. 2005; 24:232–264. [PubMed: 15389860]
15. Zhou W, Håkansson K. Structural determination of carbohydrates by fourier transform tandem mass spectrometry. Curr Proteom. 2011; 8:297–308.
16. Zaia J, McClellan JE, Costello CE. Tandem mass spectrometric determination of the 4s/6s sulfation sequence in chondroitin sulfate oligosaccharides. Anal Chem. 2001; 73:6030–6039. [PubMed: 11791576]
17. Wheeler SF, Harvey DJ. Extension of the in-gel release method for structural analysis of neutral and sialylated n-linked glycans to the analysis of sulfated glycans: application to the glycans from bovine thyroid-stimulating hormone. Anal Biochem. 2001; 296:92–100. [PubMed: 11520036]
18. Zaia J, Li XQ, Chan SY, Costello CE. Tandem mass spectrometric strategies for determination of sulfation positions and uronic acid epimerization in chondroitin sulfate oligosaccharides. J Am Soc Mass Spectrom. 2003; 14:1270–1281. [PubMed: 14597117]
19. Naggar EF, Costello CE, Zaia J. Competing fragmentation processes in tandem mass spectra of heparin-like glycosaminoglycans. J Am Soc Mass Spectrom. 2004; 15:1534–1544. [PubMed: 15519220]
20. Yu GL, Zhao X, Yang B, Ren SM, Guan HS, Zhang YB, Lawson AM, Chai WG. Sequence determination of sulfated carrageenan-derived oligosaccharides by high-sensitivity negative-ion electrospray tandem mass spectrometry. Anal Chem. 2006; 78:8499–8505. [PubMed: 17165845]
21. Desaire H, Leary JA. Detection and quantification of the sulfated disaccharides in chondroitin sulfate by electrospray tandem mass spectrometry. J Am Soc Mass Spectrom. 2000; 11:916–920. [PubMed: 11014453]
22. Kailemia MJ, Li LY, Ly M, Linhardt RJ, Amster IJ. Complete mass spectral characterization of a synthetic ultralow-molecular-weight heparin using collision-induced dissociation. Anal Chem. 2012; 84:5475–5478. [PubMed: 22715938]
23. Domon B, Costello CE. A systematic nomenclature for carbohydrate fragmentations in FAB-MS/MS spectra of glycoconjugates. Glycoconj J. 1988; 5:397–409.
24. Budnik BA, Haselmann KF, Zubarev RA. Electron detachment dissociation of peptide di-anions: an electron–hole recombination phenomenon. Chem Phys Lett. 2001; 342:299–302.
25. Yang J, Mo J, Adamson JT, Håkansson K. Characterization of oligodeoxynucleotides by electron detachment dissociation Fourier transform ion cyclotron resonance mass spectrometry. Anal Chem. 2005; 77:1876–1882. [PubMed: 15762599]
26. Adamson JT, Håkansson K. Electron detachment dissociation of neutral and sialylated oligosaccharides. J Am Soc Mass Spectrom. 2007; 18:2162–2172. [PubMed: 17962039]
27. Huzarska M, Ugalde I, Kaplan DA, Hartmer R, Easterling ML, Polfer NC. Negative electron transfer dissociation of deprotonated phosphopeptide anions: choice of radical cation reagent and

competition between electron and proton transfer. Anal Chem. 2010; 82:2873–2878. [PubMed: 20210298]

28. Zhang JH, Schubothe K, Li BS, Russell S, Lebrilla CB. Infrared multiphoton dissociation of O-linked mucin-type oligosaccharides. Anal Chem. 2005; 77:208–214. [PubMed: 15623298]
29. Wolff JJ, Chi L, Linhardt RJ, Amster IJ. Distinguishing glucuronic from iduronic acid in glycosaminoglycan tetrasaccharides by using electron detachment dissociation. Anal Chem. 2007; 79:2015–2022. [PubMed: 17253657]
30. Wolff JJ, Laremore TN, Busch AM, Linhardt RJ, Amster IJ. Electron detachment dissociation of dermatan sulfate oligosaccharides. J Am Soc Mass Spectrom. 2008; 19:294–304. [PubMed: 18055211]
31. Wolff JJ, Laremore TN, Busch AM, Linhardt RJ, Amster IJ. Influence of charge state and sodium cationization on the electron detachment dissociation and infrared multiphoton dissociation of glycosaminoglycan oligosaccharides. J Am Soc Mass Spectrom. 2008; 19:790–798. [PubMed: 18499037]
32. Wolff JJ, Laremore TN, Leach FE, Linhardt RJ, Amster IJ. Electron capture dissociation, electron detachment dissociation and infrared multiphoton dissociation of sucrose octasulfate. Eur J Mass Spectrom. 2009; 15:275–281.
33. Wolff JJ, Amster IJ, Chi L, Linhardt RJ. Electron detachment dissociation of glycosaminoglycan tetrasaccharides. J Am Soc Mass Spectrom. 2007; 18:234–244. [PubMed: 17074503]
34. Wolff JJ, Leach FE, Laremore TN, Kaplan DA, Easterling ML, Linhardt RJ, Amster IJ. Negative electron transfer dissociation of glycosaminoglycans. Anal Chem. 2010; 82:3460–3466. [PubMed: 20380445]
35. Aguilan JT, Dayrit FM, Zhang JH, Ninonuevo MR, Lebrilla CB. Structural Analysis of α-carrageenan sulfated oligosaccharides by positive mode Nano-ESI-FTICR-MS and MS/MS by SORI-CID. J Am Soc Mass Spectrom. 2006; 17:96–103. [PubMed: 16352442]
36. Liu H, Håkansson K. Electron capture dissociation of tyrosine O-sulfated peptides complexed with divalent metal cations. Anal Chem. 2006; 78:7570–7576. [PubMed: 17073428]
37. Harvey DJ. Ionization and collision-induced fragmentation of N-linked and related carbohydrates using divalent cations. J Am Soc Mass Spectrom. 2001; 12:926–937. [PubMed: 11506225]
38. Cancilla MT, Wang AW, Voss LR, Lebrilla CB. Fragmentation reactions in the mass spectrometry analysis of neutral oligosaccharides. Anal Chem. 1999; 71:3206–3218. [PubMed: 10450162]
39. Sible EM, Brimmer SP, Leary JA. Interaction of first row transition metals with a1-2, a1-6 mannotriose and conserved trimannosyl core oligosaccharides: a comparative electrospray ionization study of doubly and singly charged complexes. J Am Soc Mass Spectrom. 1997; 8:32–42.
40. König S, Leary JA. Evidence for linkage position determination in cobalt coordinated pentasaccharides using ion trap mass spectrometry. J Am Soc Mass Spectrom. 1998; 9:1125–1134. [PubMed: 9794083]
41. Hofmeister GE, Zhou Z, Leary JA. Linkage position determination in lithium-cationized disaccharides: tandem mass spectrometry and semi-empirical calculations. J Am Chem Soc. 1991; 113:5964–5970.
42. Devakumar A, Mechref Y, Kang P, Novotny MV, Reilly JP. Identification of isomeric *N*-glycan structures by mass spectrometry with 157 nm laser-induced photofragmentation. J Am Soc Mass Spectrom. 2008; 19:1027–1040. [PubMed: 18487060]
43. Xie YM, Lebrilla CB. Infrared multiphoton dissociation of alkali metal-coordinated oligosaccharides. Anal Chem. 2003; 75:1590–1598. [PubMed: 12705590]
44. Lancaster KS, An HJ, Li BS, Lebrilla CB. Interrogation of N-linked oligosaccharides using infrared multiphoton dissociation in FT-ICR mass spectrometry. Anal Chem. 2006; 78:4990–4997. [PubMed: 16841922]
45. An HJ, Miyamoto S, Lancaster KS, Kirmiz C, Li B, Lam KS, Leiserowitz GS, Lebrilla CB. Profiling of glycans in serum for the discovery of potential biomarkers for ovarian cancer. J Proteome Res. 2006; 5:1626–1635. [PubMed: 16823970]

46. Pikulski M, Hargrove A, Shabbir SH, Anslyn EV, Brodbelt JS. Sequencing and characterization of oligosaccharides using infrared multiphoton dissociation and boronic acid derivatization in a quadrupole ion trap. J Am Soc Mass Spectrom. 2007; 18:2094–2106. [PubMed: 17936010]
47. Harvey DJ, Naven TJP, Kuster B, Bateman RH, Green MR, Critchley G. Comparison of fragmentation modes for the structural determination of complex oligosaccharides ionized by matrix-assisted laser desorption/ionization mass spectrometry. Rapid Commun Mass Spectrom. 1995; 9:1556–1561. [PubMed: 8652879]
48. Harvey DJ, Bateman RH, Green BN. High-energy collision-induced fragmentation of complex oligosaccharides ionized by matrix-assisted laser desorption/ionization mass spectrometry. J Mass Spectrom. 1997; 32:167–187. [PubMed: 9102200]
49. Yu S, Wu S, Khoo K. Distinctive characteristics of MALDI-Q/TOF and TOF/TOF tandem mass spectrometry for sequencing of permethylated complex type N-glycans. Glycoconj J. 2006; 23:355–369. [PubMed: 16897178]
50. Devakumar A, Thompson MS, Reilly JP. Fragmentation of oligosaccharide ions with 157 nm vacuum ultraviolet light. Rapid Commun Mass Spectrom. 2005; 19:2313–2320. [PubMed: 16034827]
51. Devakumar A, Mechref Y, Kang P, Novotny MV, Reilly JP. Laser-induced photofragmentation of neutral and acidic glycans inside an ion-trap mass spectrometer. Rapid Commun Mass Spectrom. 2007; 21:1452–1460. [PubMed: 17385789]
52. McFarland MA, Marshall AG, Hendrickson CL, Nilsson CL, Fredman P, Mansson JE. Structural characterization of the GM1 ganglioside by infrared multiphoton dissociation/electron capture dissociation, and electron detachment dissociation electrospray ionization FT-ICR MS/MS. J Am Soc Mass Spectrom. 2005; 16:752–762. [PubMed: 15862776]
53. Budnik BA, Haselmann KF, Elkin YN, Gorbach VI, Zubarev RA. Applications of electron-ion dissociation reactions for analysis of polycationic chitooligosaccharides in Fourier Transform mass spectrometry. Anal Chem. 2003; 75:5994–6001. [PubMed: 14588042]
54. Adamson JT, Håkansson K. Electron capture dissociation of oligosaccharides ionized with alkali, alkaline earth, and transition metals. Anal Chem. 2007; 79:2901–2910. [PubMed: 17328529]
55. Zhao C, Xie B, Chan SY, Costello CE, O'Connor PB. Collisionally activated dissociation and electron capture dissociation provide complementary structural information for branched permethylated oligosaccharides. J Am Soc Mass Spectrom. 2008; 19:138–150. [PubMed: 18063385]
56. Liu HC, Håkansson K. Electron capture dissociation of divalent metal-adducted sulfated oligosaccharides. Int J Mass Spectrom. 2011; 305:170–177.
57. Tsybin YO, Witt M, Baykut G, Kjeldsen F, Håkansson P. Combined infrared multiphoton dissociation and electron capture dissociation with a hollow electron beam in Fourier transform ion cyclotron resonance mass spectrometry. Rapid Commun Mass Spectrom. 2003; 17:1759–1768. [PubMed: 12872281]
58. Caravatti P, Allemann M. The infinity cell—a new trapped ion cell with radiofrequency covered trapping electrodes for Fourier transform ion cyclotron resonance mass spectrometry. Org Mass Spectrom. 1991; 26:514–518.
59. Horn DM, Ge Y, McLafferty FW. Activated ion electron capture dissociation for mass spectral sequencing of larger (42 kDa) proteins. Anal Chem. 2000; 72:4778–4784. [PubMed: 11055690]
60. Senko MW, Canterbury JD, Guan S, Marshall AG. A high-performance modular data system for FT-ICR mass spectrometry. Rapid Commun Mass Spectrom. 1996; 10:1839–1844. [PubMed: 8953786]
61. Ledford EB Jr, Rempel DL, Gross ML. Space Charge effects in fourier transform mass spectrometry mass calibration. Anal Chem. 1984; 56:2744–2748. [PubMed: 6524653]
62. Lohmann KK, von der Lieth CW. GlycoFragment and GlycoSearchMS: Web tools to support the interpretation of mass spectra of complex carbohydrates. Nucleic Acids Res. 2004; 32:W261–W266. [PubMed: 15215392]
63. Green ED, Baenziger JU. Asparagine-linked oligosaccharides on lutropin, follitropin, and thyrotropin. 1. Stuctural elucidation of the sulfated and sialylated oligosaccharides on bovine,

ovine, and human pituitary glycoprotein hormones. J Biol Chem. 1988; 263:25–35. [PubMed: 3121609]

64. Håkansson K, Cooper HJ, Emmett MR, Costello CE, Marshall AG, Nilsson CL. Electron capture dissociation and infrared multiphoton dissociation MS/MS of an N-glycosylated tryptic peptide yield complementary sequence information. Anal Chem. 2001; 73:4530–4536. [PubMed: 11575803]
65. Stensballe A, Norregaard-Jensen O, Olsen JV, Haselmann K, Zubarev RA. Electron capture dissociation of singly and multiply phosphorylated peptides. Rapid Commun Mass Spectrom. 2000; 14:1793–1800. [PubMed: 11006587]
66. Shi SDH, Hemling ME, Carr SA, Horn DM, Lindh I, McLafferty FW. Phosphopeptide/phosphoprotein mapping by electron capture dissociation mass spectrometry. Anal Chem. 2001; 73:19–22. [PubMed: 11195502]
67. Håkansson K, Chalmers MJ, Quinn JP, McFarland MA, Hendrickson CL, Marshall AG. Combined electron capture and infrared multiphoton dissociation for multistage MS/MS in an FT-ICR mass spectrometer. Anal Chem. 2003; 75:3256–3262. [PubMed: 12964777]
68. Håkansson K, Hudgins RR, Marshall AG, O'Hair RAJ. Electron capture dissociation and infrared multiphoton dissociation of oligodeoxynucleotide dications. J Am Soc Mass Spectrom. 2003; 14:23–41. [PubMed: 12504331]
69. Yang J, Håkansson K. Fragmentation of oligoribonucleotides from gas-phase ion-electron reactions. J Am Soc Mass Spectrom. 2006; 17:1369–1375. [PubMed: 16872836]
70. Ge Y, Lawhorn BG, ElNaggar M, Strauss E, Park JH, Begley TP, McLafferty FW. Top down characterization of larger proteins (45 kDa) by electron capture dissociation mass spectrometry. J Am Chem Soc. 2002; 124:672–678. [PubMed: 11804498]
71. Penn SG, Cancilla MT, Lebrilla CB. Collision-induced dissociation of branched oligosaccharide ions with analysis and calculation of relative dissociation thresholds. Anal Chem. 1996; 68:2331–2339. [PubMed: 8686926]

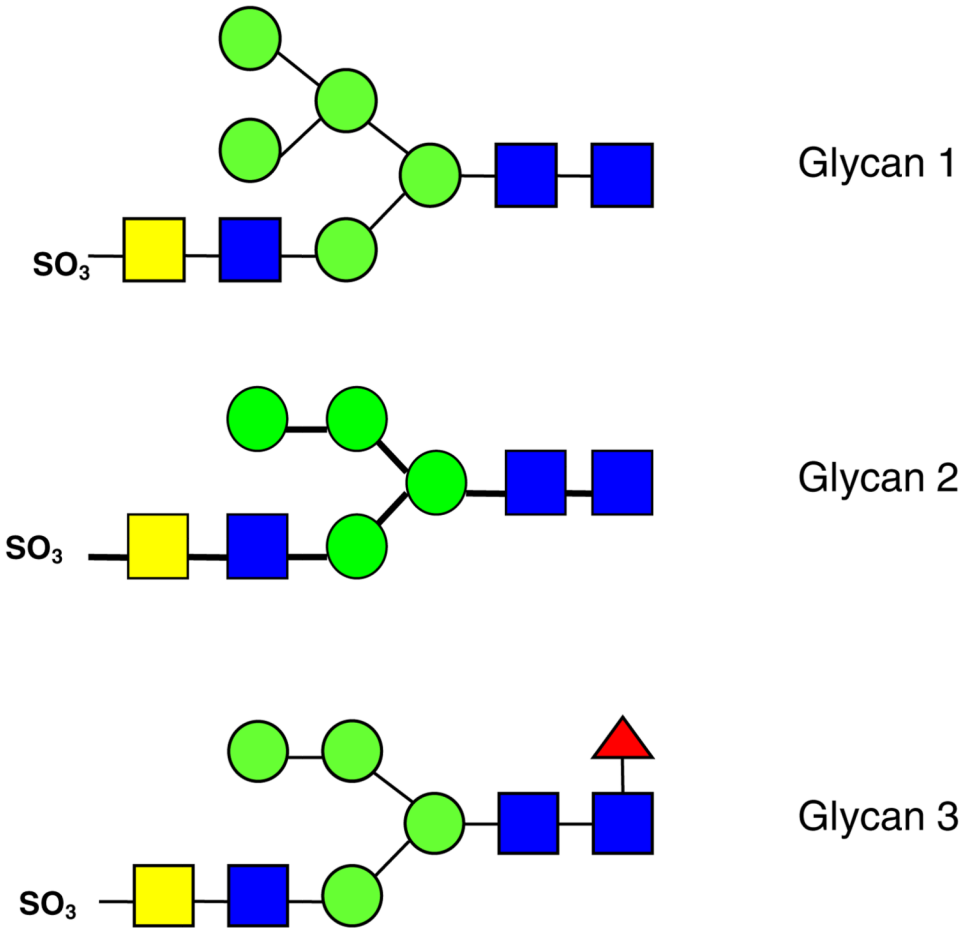

Figure 1. Sulfated *N*-glycans released from bovine thyroid stimulating hormone ●: mannose, □: *N*-acetylglucosamine (GlcNAc), ▲: fucose, ■: *N*-acetylgalactosamine (GalNAc)

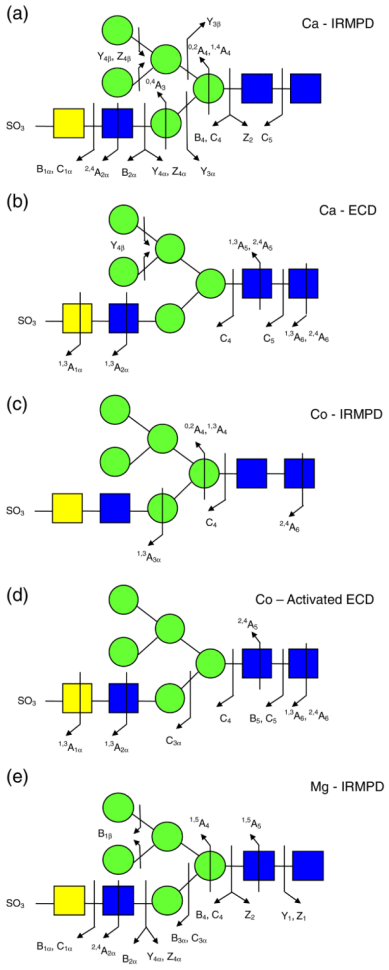

Figure 2.

Fragmentation patterns of metal-adducted *N*-glycan 1. **(a)** IRMPD of calcium adduct (40 scans, 50 ms irradiation, 10 W laser power); **(b)** ECD of calcium adduct (40 scans, 80 ms electron irradiation with a bias voltage of −0.2 V); **(c)** IRMPD of cobalt adduct (40 scans, 40 ms irradiation, 10 W laser power); **(d)** AI-ECD of cobalt adduct (40 scans, 15 ms irradiation with 10 W laser power, 80 ms electron irradiation with a bias voltage of −0.15 V); **(e)** IRMPD of magnesium adduct (40 scans, 50 ms irradiation, 10 W laser power)

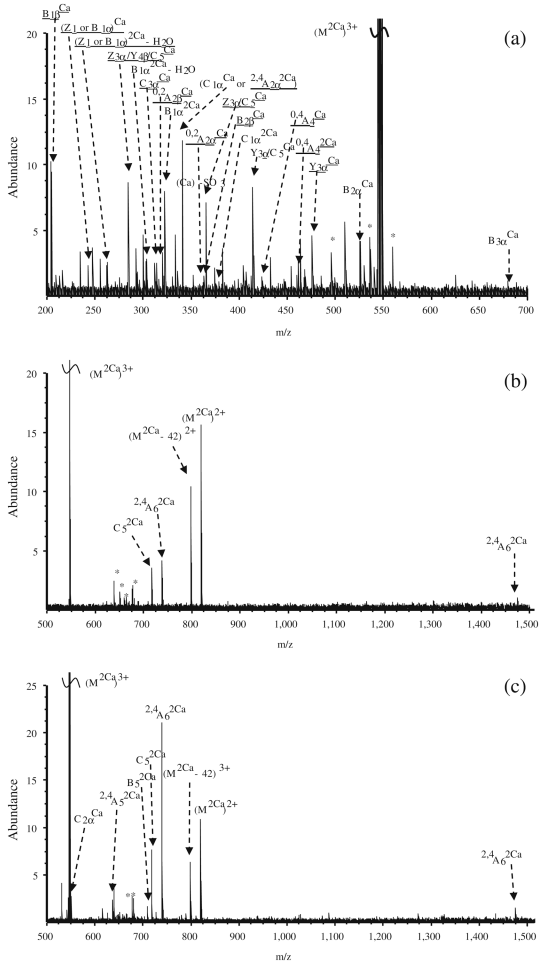

Figure 3.

FT-ICR tandem mass spectra of Ca^{2+}-adducted *N*-glycan 2. **(a)** IRMPD (40 scans, 80 ms irradiation, 10 W laser power); **(b)** ECD (50 scans, 50 ms electron irradiation with a bias voltage of −0.2 V); **(c)** AI-ECD (40 scans, 20 ms irradiation with 10 W laser power, 100 ms electron irradiation with a bias voltage of −0.25 V). Product ions are underlined if they underwent sulfonate loss. The superscript ‘Ca’ indicates product ions bearing a calcium cation. Assignments indicated in bold are crossring product ions. * Denotes electronic noise

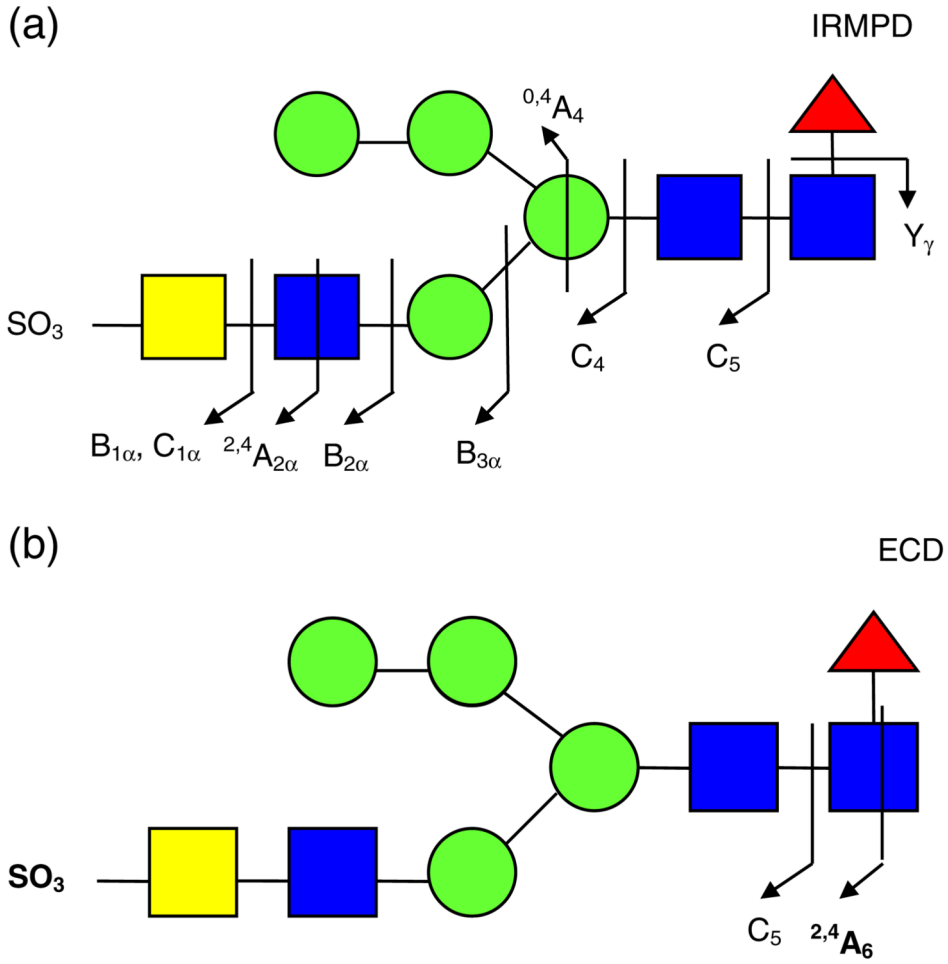

Figure 4. Fragmentation patterns of Ca^{2+}-adducted *N*-glycan 3. (a) IRMPD (40 scans, 50 ms irradiation, 10 W laser power); (b) ECD (64 scans, 50 ms electron irradiation with a bias voltage of −0.3 V)

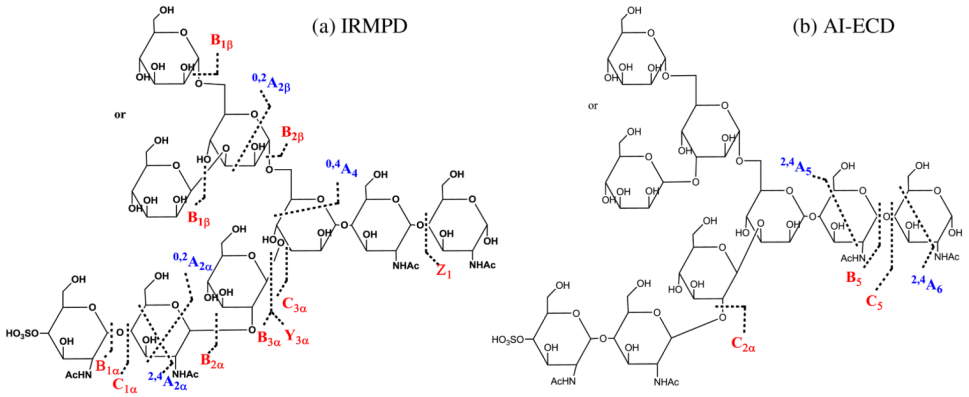

Scheme 1. Fragmentation patterns of Ca^{2+}-adducted N-glycan 2. (a) IRMPD and (b) AI-ECD. Glycosidic cleavages are labeled in red. Cross-ring cleavages are labeled in blue. Internal fragments are not shown